Integrated Histology and Molecular Profiling of Postmortem Human Auditory and Vestibular Organs via a Poly(Methyl Methacrylate)-Based Workflow

Authors

David Bächinger (1,2), Brock Peyton (3,4,5), Jacqueline Neubauer (6), Anbuselvan Dharmarajan (3,4,5), MengYu Zhu (3,4,5), Jennifer T. O'Malley (3,4,5), Venus Kallupurackal (6), Steven Senese (7), Alison Brown (8), Sabina Wunderlin (9), Susanne Kreutzer (10), Nora M. Weiss (11, 12), Heiko Richter (13), Adrian Dalbert (1,2), Christof Röösli (1,2), Anja Kipar (9), Zsuzsanna Varga (14), Brigitte von Rechenberg (15), Sami S. Amr (8,16), Andreas H. Eckhard (3,4,5,*)

Affiliations

(1) Department of Otorhinolaryngology, Head and Neck Surgery, University Hospital Zurich, Zurich, Switzerland

(2) University of Zurich, Zurich, Switzerland

(3) Otopathology Laboratory, Mass Eye and Ear, MA, USA

(4) Eaton-Peabody Laboratories, Massachusetts Eye and Ear, Boston, MA, USA

(5) Department of Otolaryngology, Harvard Medical School, Boston, MA, USA

(6) Zurich Institute of Forensic Medicine, University of Zurich, Zurich, Switzerland

(7) Department of Epidemiology, Harvard T.H. Chan School of Public Health, Boston, MA, USA

(8) Laboratory for Molecular Medicine, Personalized Medicine, Mass General Brigham, Cambridge, MA, USA

(9) Department of Pathobiology, Institute of Veterinary Pathology, Vetsuisse Faculty, University of Zurich, Zurich, Switzerland

(10) Functional Genomics Center Zurich, ETH Zurich and University of Zurich, Zurich, Switzerland.

(11) Department of Otorhinolaryngology, Head and Neck Surgery “Otto Körner”, University Medical Center, Rostock, Germany

(12) Department of Otolaryngology Head and Neck Surgery, School of Medicine, Technical University of Munich, Munich, Germany

(13) LLS Rowiak LaserLabSolutions GmbH, Hannover, Germany

(14) Department of Pathology and Molecular Pathology, University Hospital Zurich, Zurich, Switzerland

(15) Musculoskeletal Research Unit, Vetsuisse Faculty, University of Zurich, Switzerland

(16) Department of Pathology, Brigham and Women's Hospital, Harvard Medical School, Boston, MA, USA

* Corresponding author

Address for correspondence

Andreas H. Eckhard, MD

Otopathology Laboratory, Department of Otolaryngology

Massachusetts Eye and Ear

243 Charles Street, Boston, MA 02114, USA

Phone: +1 (617) 573-3875

Email: aeckhard@meei.harvard.edu

Conflicts of interest and funding

The authors report no conflicts of interest. This work was supported in part by MED-EL (Innsbruck, Austria), which had no involvement in study design, data collection, analysis, interpretation, or manuscript preparation.

Abstract

Hearing and balance disorders are the most prevalent sensory impairments, affecting hundreds of millions worldwide, yet their underlying cellular and molecular pathologies remain poorly understood. This knowledge gap stems from the inaccessibility of the ear's sensory organs—embedded within the temporal bone (TB), the hardest bone in the body—which cannot be biopsied in living patients without causing irreversible damage. Conventional histopathology workflows rely on postmortem en bloc extraction of TBs, followed by lengthy decalcification, celloidin embedding, and manual serial sectioning of these large specimens—a process that takes one to two years, is labor- and cost-intensive, and lacks compatibility with most modern protein, DNA, and RNA assays. Here, we present a rapid, reversible polymethyl methacrylate (rPMMA) workflow that enables advanced molecular histopathology studies on formalin-fixed, calcified, TBs. Our protocol uses low-temperature (–40 °C to +4 °C) resin embedding, precision near-serial sectioning (10–50 µm) via femtosecond laser microtomy or precision diamond wire sawing, and subsequent deacrylation to fully restore tissue accessibility for high-fidelity histomorphology, multiplexed immunofluorescence, whole-genome sequencing, and in situ mRNA detection (RNAscope™) assays. Compared to the gold-standard celloidin workflow, our method reduces processing time and costs by approximately 90% while integrating equivalent histomorphology with advanced molecular assays, providing a new benchmark for multidimensional studies in human hearing and balance pathologies.

Key words

inner ear, celloidin, Technovit® 9100, immunohistochemistry, reversible poly methyl methacrylate, DNA, laser microtomy, RNAscope

Introduction

Hearing and balance disorders are the leading global causes of sensory impairment[1–3], yet their underlying cellular and molecular pathologies remain poorly understood—a major barrier to new therapeutic development[4]. This knowledge gap stems from the inaccessibility of the ear's sensory organs, which lie embedded within the skull's temporal bone (TB)—the hardest bone in the human body—and cannot be biopsied in vivo without causing irreversible damage. Consequently, human pathology studies on hearing and balance disorders rely almost exclusively on en bloc TB specimens harvested postmortem from individuals with well-documented clinical histories[5,6].

Human TB specimens containing the ear's sensory structures are large (approximately 38 × 38 × 50 mm[5,7]) and anatomically complex, with delicate sensory tissues suspended in air- and fluid-filled chambers encased by densely mineralized bone. Standard histology workflows—using cryomedia[8,9], paraffin[8,10], polyester wax[11], or hard resins (Epon[12,13], araldite[14])—either introduce substantial artifacts that distort fine structure to the point of being uninterpretable, necessitate specimen downsizing that removes key sensory structures, or irreversibly lock tissue within the embedding matrix, precluding downstream molecular assays[10,14]. Over a century ago, nitrocellulose (celloidin) embedding[15] became the gold standard for whole-TB histology[16–18], preserving pristine light-microscopic morphology in intact, full-size specimens. Celloidin-based studies of the human hearing and balance organs laid the groundwork for defining their pathologies[17–20], and later refinements enabled gentle celloidin removal for first immunohistochemical protein localization studies[21–25]—though these protocols remain applicable only in a limited manner. Overall, the "celloidin workflow" ranges from technically challenging to incompatible with multiplex immunohistochemistry[26], RNA in situ hybridization, and sequencing-based assays[27–29], and few, if any, studies have demonstrated these applications on celloidin-processed human TB sections. Moreover, it requires at least

13.5 months, including 2–3 weeks of fixation, up to 36 weeks of decalcification, 2 weeks of dehydration, 18 weeks of embedding, followed by serial sectioning of approximately 450 sections (20 μm thick) on heavy sledge microtomes[30], and is both resource- and labor-intensive, with constant supply challenges for celloidin.

To overcome these barriers, we re-engineered the histology workflow for whole human TB specimens around three core objectives: (1) enhance preservation and accessibility of proteins, DNA, and RNA for molecular assays; (2) maintain celloidin-level (gold-standard) histomorphological fidelity for meaningful interpretation at tissue and cell level; and (3) reduce processing time, complexity, and cost to facilitate broad adoption, as well as streamlined section archiving and distribution. Central to our novel approach is a reversible polymethyl methacrylate (rPMMA) resin embedding workflow that leverages controlled low-temperature conditions (-40 °C to +4 °C) and eliminates months-long decalcification. After embedding, calcified specimens are sectioned near-serially (10–50 μm) via femtosecond laser microtomy or precision diamond-wire sawing, then fully deacrylated (rPMMA resin removed) from mounted tissue sections. This approach preserves exceptional histomorphology of whole human TB specimens, restores antigenicity for multiplexed immunofluorescence labeling, and preserves nucleic acid integrity for whole-genome sequencing and in situ RNA detection (e.g., RNAscope™). By addressing longstanding technical obstacles posed by human TB anatomy, our rPMMA-based workflow offers a new benchmark for multidimensional studies in human ear pathology.

Materials and methods

Ethics

This study was approved by the Institutional Review Boards of Massachusetts Eye and Ear (Boston, USA; #2021P001593), University Hospital Zurich (Zurich, Switzerland; #BASEC-2021-00820), and University Hospital Rostock (Rostock, Germany; #A-2020-0264). Written informed consent was obtained from all tissue donors or their legal representatives.

Specimen harvesting and preparation

TB specimens were harvested using the intracranial bone plug technique[30]. Briefly, following craniectomy, a cylindrical bone plug containing the ear structures was removed using an oscillating autopsy saw (810 autopsy saw, Stryker, Kalamazoo, MI; 3.8 cm diameter trephine; see [30]) (Figure 1A, harvesting). The study included seven TBs from adult donors (aged 56–78 years; postmortem interval 4–40 hours). Skeletal muscle (fresh frozen) from one donor was used as a sequencing control. Additionally, archival tissue sections from four donors, originally processed using the celloidin embedding protocol and stored in 80% ethanol, were included as controls for histomorphological analysis, DNA extraction, and RNA in situ hybridization. These specimens were selected based on matched postmortem intervals, with priority given to those with the shortest ethanol storage duration.

Harvested specimens were immediately placed in ice-chilled 10% neutral buffered formalin for laboratory transfer. Excess bone on each specimen side was trimmed using a tabletop pathology bandsaw (#BBS-82203, IMEB Inc., San Marcos, CA) equipped with a diamond blade (#SD311, IMEB Inc.), reducing dimensions to approximately 35×25×25 mm (Figure 1A, trimming). Dura mater was removed, and the bone covering the superior semicircular canal was carefully drilled (#4-6 diamond burr; Figure 1A, drilling) and finally

opened it with a bone curette to facilitate formalin penetration and avoid scattering bone debris from drilling into the inner ear spaces.

Fixation and dehydration

Specimens were fixed in 10% formalin at 4°C for 6 days, then dehydrated through a graded ethanol series (30%, 70%, 80%, 95%, 100% ethanol; 24 hours each), followed by two cycles each of absolute ethanol and xylene (#X5-4, Fisher Scientific, Waltham, MA) or Histo-Clear™ (#HS-200, National Diagnostics, Atlanta, GA), 24 hours per cycle.

rPMMA resin embedding

Embedding of TB specimens was performed using the reversible (i.e., deacrylatable to free embedded and sectioned tissue) polymethyl methacrylate (rPMMA) resin system Technovit® 9100 (#64715444, Kulzer GmbH, Hanau, Germany, or #813-900, Ted Pella Inc., Redding, CA), following the manufacturer's recommendations. *Preparation of solutions*: All embedding solutions were freshly prepared and stored at -20°C until use. Destabilized base solution (BS): The base solution was destabilized by passage through a chromatography column (53 mm × 457 mm; PTFE stopcock, #31-500-983, Fisher Scientific) filled with 50 g aluminum oxide (#AA4717136, Fisher Scientific). Pre-infiltration Solutions (PIS) 1: Mixture of 100 ml xylene (or Histo-Clear™) and 100 ml stabilized BS. PIS 2: 0.5 g hardener 1 dissolved in 200 ml stabilized BS. PIS 3: 0.5 g hardener 1 dissolved in 200 ml destabilized BS. Infiltration Solution (IS): 0.5 g hardener 1 and 16 g PMMA dissolved in 200 ml destabilized BS. PMMA powder was slowly added and stirred for 2–4 hours to ensure complete dissolution. Polymerization Solution A (PS-A): 0.4 g hardener 1 and 36.8 g PMMA in 230 ml destabilized BS, stirred 2–4 hours for full dissolution. Polymerization Solution B (PS-B): 2 ml hardener 2 and 1 ml regulator mixed in 25 ml destabilized BS. When not in use, all solutions were stored at –

20 °C. *Infiltration protocol*: Specimens were sequentially incubated in PIS 1, PIS 2, and PIS 3, each for 3 days at 4°C, followed by IS for 4 days at 4°C and then at -40°C for an additional day. During transitions between solutions, specimens were gently rotated to release trapped gas bubbles and handled with non-metal (polyoxymethylene) forceps (#BR112805, Millipore-Sigma, Burlington, MA). *Polymerization protocol*: Polymerization was performed in a benchtop freezer modified with a 1-inch rear access port (-45 °C; #2002010, Super Coldcube, Industrial Freezer Sales, Agoura Hills, CA) using a vacuum desiccator (#F42012-0000, 0.09 cu. ft.; SP Bel-Art, Wayne, NJ) connected to a wall vacuum (-500 mbar) through this port. Polymerization solutions A and B, along with all materials were pre-cooled for at least one hour to -40°C. PS-A (90 ml) and PS-B (10 ml) were mixed in a 9:1 ratio and poured into a 100 ml glass jar (#3TRF1, Grainger, Lake Forest, IL). The specimen was carefully immersed, rotated gently to release trapped gas bubbles, and placed in the desiccator inside the benchtop freezer. Polymerization occurred at -40°C under -500 mbar vacuum for three days, with daily brief interruptions to rotate specimens and release gas bubbles. On day three, the specimen was positioned in its final orientation (tegmen down) and a 5 mm layer of paraffin oil (#MPX00461, Fisher Scientific) was added atop the polymerization solution to exclude oxygen, critical for complete polymerization. Temperature was gradually increased by increments of 5°C every three days until -15°C, maintaining a -500 mbar vacuum. After three days at –15 °C, the glass jar containing the specimen was moved to a refrigerator and held at 4 °C (without vacuum) for one further day. The paraffin oil was then drained, and the polymerized specimen was carefully freed by fracturing the jar with a hammer. See Supplementary material 1 (“Technovit® 9100 Embedding Protocol for Calcified Human Temporal Bones”) for a detailed lab version. All rPMMA-processed TB specimens were labeled sequentially as TV 1 through TV 7, according to their specimen number.

High resolution peripheral quantitative computed tomography (HR-pQCT) imaging

TB specimens embedded in rPMMA were scanned using an XtremeCT II HR-pQCT system (Scanco Medical, Brütisellen, Switzerland). Imaging was performed at an isotropic voxel resolution of either 61 μm^3 or 82 μm^3. The scan parameters included an x-ray tube potential of 68 kVp, x-ray tube intensity of 147 mA, and integration time of 100 milliseconds. The acquired DICOM datasets were subsequently imported into 3D Slicer software (version 5.6.1; https://www.slicer.org). The anatomical plane representing the longitudinal axis through the cochlea's modiolus was defined. Fiducial markers (sticky tape) indicating this mid-modiolar plane were placed directly on the surface of each embedded specimen.

Histological sectioning

Resin blocks with embedded human TBs were first trimmed to a 25 mm maximum width to fit standard microscope slides and cut along the cochlear midmodiolar plane (see previous paragraph), using a tabletop bandsaw ((#BBS-82203, IMEB Inc.) fitted with a diamond saw blade (#SD311, IMEB Inc.), and operated with water irrigation to prevent thermal damage of the resin and specimen. The block's cut surface was then smoothed using a disc sander (TG 125/E, Proxxon, Hickory, NC) with 600 grit sanding discs. Finally, each block was mounted—cut side down—onto a plain microscope slide (#12-550-10; Fisher Scientific) with a transparent, rapid-set two-component epoxy (Araldite Crystal Clear, Huntsman Advanced Materials).

Sections 20–50 μm thick were prepared using one of three methods. *Laser microtomy*: Mounted blocks were positioned on the motorized stage of a TissueSurgeon device (LLS ROWIAK LaserLabSolutions, Hannover, Germany). A femtosecond laser (1030 nm wavelength, 300 fs pulse duration, 10 MHz repetition rate) was focused from beneath through a microscope slide, penetrating 20 μm into the specimen to evaporate resin and embedded tissue. Sections were produced within 10-15 minutes and subsequently polished. *Precision*

147 *diamond wire sawing*: Specimen blocks were secured in a standard holder of a diamond wire
148 saw device (DWS.100, Diamond WireTec, Weinheim, Germany). Sections were cut using a 50
149 µm thin diamond-coated steel wire (#DW050T, Diamond WireTec) at a maximum speed of 4
150 m/s, yielding approx. 50 µm thick sections within 10-15 minutes without requiring polishing.
151 *Tabletop bandsaw and disk sander*: Blocks were guided along a straight-edge guide through
152 tabletop band saw (#BBS-82203, IMEB Inc.) fitted with a diamond saw blade (#SD311, IMEB
153 Inc.), producing sections approximately 300 µm thick. These were thinned and polished to a
154 final thickness of about 50 µm using a disc sander (TG 125/E, Proxxon) with a 2000 grit sanding
155 disc. After each cut, the blocks were remounted and the sectioning procedure repeated to
156 generate additional 20–50 µm sections.
157
158 *Deacrylating mounted hTB sections*
159 For subsequent immunohistochemistry, DNA extraction, or in situ RNA labeling mounted
160 sections were deacrylated by placing the slides—tissue side down—in a glass staining jar filled
161 with 2-methoxyethyl acetate (2-MEA; #M011325ML, Fisher Scientific) for 30 minutes, allowing
162 the dissolved resin to drip away by gravity. Sections were then rehydrated sequentially in xylene
163 (or Histo-Clear™), graded ethanol solutions, distilled water, and finally PBS, each for 10
164 minutes.
165
166 *Archival, celloidin-processed TB sections*
167 Celloidin-processed TB specimens, archived at Mass Eye and Ear (Boston, USA) and
168 the University Hospital Zurich (Zurich, Switzerland) and designated sequentially as CL 1
169 through CL 3, were used as controls to benchmark histomorphological preservation and DNA
170 extraction quality. Specimens were fixed in 10% neutral buffered formalin for 7–10 days,
171 decalcified in 0.27 M ethylenediaminetetraacetic acid (EDTA; #S311-3, Fisher Scientific) for

172 approximately 270–450 days depending on specimen size, and dehydrated in a graded ethanol
173 series for 10 days. Embedding was performed over 84 days using increasing concentrations
174 (up to 12%) of celloidin (nitrocellulose; LADD Research, Williston, VT, #10838) dissolved in a
175 1:1 mixture of absolute ethanol and ethyl ether (#E138-1, Fisher Scientific). The final
176 embedding blocks were hardened for 14 days, followed by immersion in chloroform
177 (#C298SK4, Fisher Scientific) and cedarwood oil (Polysciences Inc., #04851-4) for two weeks
178 each prior to sectioning. Individual sections were mounted on numbered pieces of onion skin
179 paper in a dish of 80% ethanol, and stored long-term in 80% ethanol at room temperature. For
180 histomorphological comparison, archived sections from specimens most recently processed
181 and matched for postmortem interval and donor age were selected. For DNA extraction
182 experiments, the most recently archived sections from the University Hospital Zurich, stored for
183 20–21 years, were used.
184
185 *Histochemical staining*
186 Sections from rPMMA-embedded human TBs were stained using hematoxylin and eosin
187 (HE) or von Kossa methods without prior deacrylation, either manually or with an automatic
188 slide stainer (Tissue-Tek Prisma, Sysmex Europe GmbH, Norderstedt, Germany). Stained
189 sections were coverslipped using permanent mounting medium (Vectamount, #H-5000, Vector
190 Laboratories, Newark, CA; or Permount, #SP-100, Fisher Scientific).
191
192 *Enzyme immunohistochemistry and multiplexed immunofluorescence labeling*
193 Tissue sections were blocked for 15 minutes in PBS containing 5% normal horse serum
194 (NHS) and then incubated overnight at room temperature with primary antibodies (diluted 1: —
195 in 1% NHS; see Supplementary table 1 for antibody and fluorescent secondary combinations).
196 After three 10-minute PBS washes, sections were incubated for 1 hour at room temperature

197 with the appropriate secondary antibodies (also diluted in 1% NHS), followed by three additional
198 PBS rinses. For chromogenic detection, the Fast Red Substrate Kit (#ab64254, Abcam) was
199 applied per the manufacturer's instructions; these sections were then dehydrated through
200 graded ethanol, cleared in Histo-Clear, and coverslipped with Vectamount permanent mounting
201 medium (#H-5000, Vector Laboratories, Newark, CA, USA). For multiplexed
202 immunofluorescence, either fluorescently conjugated secondaries or biotinylated secondaries
203 (Vectastain ABC-HRP Kit #PK-4000, Vector Laboratories) plus a streptavidin-linked fluorescent
204 probe were used; fluorescent sections were counterstained with Hoechst 33258 (1:1,000 in
205 PBS; #H3569, Thermo Fisher) and coverslipped in Vectashield antifade medium (#H-1000-10,
206 Vector Laboratories). Negative controls omitted the primary antibody.
207
208 *DNA extraction, quantification, and quality assessment*
209 DNA was extracted from individual 20 µm tissue sections (from one TB specimen per
210 donor; samples TV 1–7). To remove the adhesive, slides were warmed to 70°C, and sections
211 were gently detached. Each section was deacrylated in 50 mL of 2-MEA for 20 minutes under
212 constant agitation, then rinsed three times in PBS for 5 minutes each. For celloidin-embedded
213 sections, tissues were immersed in methanol saturated with sodium methoxide at a 1:2 dilution
214 in methanol for 5 minutes, followed by a 100% methanol rinse at room temperature; this process
215 was repeated three times [31]. For samples TV 1–6 and CL 1–3, DNA was extracted using the
216 PrepFiler™ BTA Forensic DNA Extraction Kit (#4463352, Thermo Fisher Scientific,
217 Switzerland), a kit specifically optimized for calcified tissues and those containing adhesives.
218 DNA from sample TV 7 and its corresponding fresh frozen specimen was isolated using the
219 QIAamp® DNA FFPE Kit (#56404, Qiagen, Germantown, MD) according to manufacturer's
220 instructions. DNA quantity and quality were evaluated using the human-specific Quantifiler™
221 Trio DNA Quantification Kit (#4482910, Thermo Fisher Scientific) alongside PicoGreen dsDNA

assay kit (#P7589, Thermo Fisher Scientific) and Nanodrop spectrophotometry, ensuring consistency with established standards.

Short tandem repeat analysis

A total of 600 pg of the extracted DNA was processed using the AmpFLSTR NGM SElect PCR Amplification Kit (#4457889, Thermo Fisher Scientific), amplifying 16 autosomal short tandem repeat (STR) loci as well as the amelogenin gene (AMEL) used for gender identification (sex-typing).

DNA library preparation and whole-genome sequencing

For samples TV 1–6 and CL 1–3, genomic DNA was first sheared using a Covaris E220 focused ultrasonicator (#500239, Covaris, Woburn, MA). Libraries were then prepared with the NEBNext® Ultra™ II DNA Library Prep Kit (#E7645, New England Biolabs, Ipswich, MA). DNA overhangs were end-repaired, adenylated, and ligated to the NEB hairpin adapter. An adapted bead cleanup (1.8X) for low-input protocols was used, and the resulting libraries were amplified using unique P5 and P7 PCR primers (NEB, Ipswich, MA). Library quality and quantity were assessed with the Qubit 1.0 Fluorometer (Fisher Scientific) and Agilent TapeStation (Agilent, Waldbronn, Germany), then normalized to 10 nM in 10 mM Tris-Cl (pH 8.5) with 0.1% Tween 20. For samples TV7 and TV7-FF, DNA (1 µg input) was processed independently using the TruSeq PCR-Free library prep kit (#20015962, Illumina, San Diego, CA), following the manufacturer's guidelines. Libraries were quantified with the Qubit dsDNA HS Assay Kit (#Q32851, Invitrogen, Waltham, MA) and sized using the BioAnalyzer 2100 High Sensitivity DNA Kit (#5067-4626, Agilent, Santa Clara, CA). They were then normalized to 4 nM based on these readings and re-quantified using a qPCR assay with the KAPA Library Quantification Kit for Illumina Libraries (#KK4824, Roche, Basel, Switzerland).

247

248 *Sequencing QC and analysis*

249 The pooled libraries of the samples TV 1–6 and CL 1–3 were sequenced using a paired-
250 end read configuration with 150 bp per read using the Illumina Novaseq 6000 (Illumina, Inc,
251 San Diego, CA) and demultiplexed with bcl2fastq allowing for 1 mismatch in barcode 2. Reads
252 were quality-checked with fastqc[32] and were aligned to the human hg38 reference genome
253 using bowtie2 and default parameters. For samples TV 7 and TV 7 FF, libraries were pooled
254 and sequenced using the Illumina NovaSeq 6000 sequencing platform on a 2x150 bp paired
255 end SP flowcell (Illumina, San Diego, CA). Sequencing data was processed and analyzed using
256 the DRAGEN germline analysis pipeline, available through the Basespace Sequencing Hub
257 (https://basespace.illumina.com/). DRAGEN provides end-to-end secondary analysis including
258 mapping, alignment and variant calling (PMID: 33214604, PMID: 38260545). Sequencing reads
259 were aligned to the human hg38 reference genome and analysis was performed using
260 DRAGEN default parameters.

261

262 *In situ total RNA labeling and RNase A-mediated validation*

263 Sections were labeled in situ with either Syto RNASelect (0.5 μM; Invitrogen #S32703)
264 or StrandBrite Green RNA Dye (10 μM; AAT Bioquest #17610) diluted in DEPC-treated water,
265 incubated for 30 minutes at room temperature in the dark. After three 10-minute washes in
266 RNase-free water, nuclei were counterstained with Hoechst 33258 (1 μg/mL; #H3569, Thermo
267 Fisher) for 15 minutes, followed by three additional washes. Confocal image stacks of the spiral
268 ganglion region were acquired on a Leica SP5 with a 40× water-dipping objective (NA 1.1),
269 using sequential channels to avoid bleed-through (Syto RNASelect: 490/530 nm; StrandBrite:
270 488/520 nm; Hoechst: 405/460 nm). Without removing the slide from the stage, sections were
271 then covered with either RNase A (100 μg/mL; #EN0531, Fisher Scientific) or RNase-free water

and incubated for 3 hours at room temperature. The same field was re-imaged under identical settings, and loss of RNA-selective fluorescence versus stable Hoechst signal confirmed dye specificity.

RNAscope™ in situ hybridization

Chromogenic in situ hybridization was performed using the RNAscope™ 2.5 HD Duplex Detection Kit (#322430; Advanced Cell Diagnostics, Newark, CA, USA) according to the manufacturer's instructions. Pretreatment of 5 µm tissue sections comprised the following steps: incubation in hydrogen peroxide at room temperature for 10 minutes; heat-induced epitope retrieval in Target Retrieval Buffer in a pressure cooker within a microwave for 15 minutes; and protease Plus treatment at 40 °C for 30 minutes. Sections were then hybridized in the HybEZ Oven with the kit's positive-control probes—peptidylprolyl isomerase B (PPIB; channel 1) and RNA polymerase II subunit A (POLR2A; channel 2). After sequential amplification, PPIB was visualized with the green chromogen and POLR2A with Fast Red, yielding discrete green and red signals, respectively. Slides were briefly rinsed, dehydrated through graded ethanols, cleared in xylene, and coverslipped with Permount mounting medium (Fisher Scientific). For detection of calbindin-2 transcripts, separate serial sections underwent identical pretreatment, hybridization, and amplification using the human CALB2 probe (channel 2; #422179 Hs-CALB2, Advanced Cell Diagnostics). The CALB2 signal was developed with Fast Red.

Following RNAscope™, sections were immunofluorescently labeled for NF-h, CellMask Deep Red (#C10046, Fisher Scientific), and counterstained with Hoechst 33258. Antibody and dye dilutions, fluorophore conjugations, and incubation conditions are provided in Supplementary table 1. Finally, slides were coverslipped with ProLong™ Gold Antifade (#P36930, Fisher Scientific) mounting medium.

297

298 *Image acquisition and postprocessing*

299 Sections stained with colorimetric (enzymatic) detection methods were imaged using a
300 Nikon Eclipse E800 microscope (Nikon Instruments, Melville, NY) equipped with Nomarski
301 optics and a DS-Ri2 digital color camera (Nikon Instruments) or an Olympus BX51 microscope
302 (Olympus, Tokyo, Japan) equipped with a DP70 digital color camera (Olympus).
303 Immunofluorescence labeled sections were imaged using a Leica TCS SP8 confocal
304 microscope (Leica Microsystems GmbH, Wetzlar, Germany).

305

306 *RNAscope™ signal quantification*

307 Images of primary vestibular (Scarpa's ganglion neurons were acquired showing
308 chromogenic CALB2 (red) and fluorescent NF-h, CellMask™ Deep Red, and Hoechst 33258
309 signals. In Dragonfly software (v.2024.1, Comet Technologies, Montreal, Canada), the CALB2
310 and NF-h channels were loaded and each converted to a binary mask using Otsu thresholding
311 (with a lower threshold for CALB2 and a higher one for NF-h). NF-h fluorescence signal not
312 associated with vestibular ganglion cell soma was manually removed, and individual NF-h–
313 positive ganglion cell ROIs were defined. A Boolean "AND" operation between the CALB2 and
314 NF-h masks then quantified the CALB2-positive pixels within each NF-h–positive soma. Finally,
315 for each cell, CALB2-positive area was expressed as a percentage of its total NF-h–positive
316 area.

317

318 *Statistics*

319 Quantitative data are reported as mean ± standard deviation (SD) unless otherwise
320 specified. Normality of distribution was assessed using the Shapiro–Wilk test. For comparisons
321 between two groups, an unpaired two-tailed Student's t-test was used; for paired

measurements of fluorescence intensity before and after RNase A treatment a paired t-test was applied. Statistical analyses were performed in GraphPad Prism 9.0 (GraphPad Software, San Diego, CA), with a two-tailed $p < 0.05$ considered significant. Exact n (biological and technical replicates) and p values are indicated in the figure legends.

Results

Improved processing efficiency and cost savings

The novel rPMMA method (Figure 1A) dramatically accelerates and reduces the cost of human TB processing compared with the traditional celloidin workflow. Whereas celloidin processing—from initial fixation to complete embedding—required on average 17.3 months, rPMMA shortens this timeline to just 1.8 months by eliminating the prolonged EDTA decalcification step and utilizing a faster resin polymerization process (Figure 1B). Correspondingly, per-specimen costs fall from approximately USD 1,577 with celloidin to USD 140 using rPMMA (Figure 1C). These advantages are partially offset during the sectioning stage. Unlike decalcified, celloidin-embedded TBs, calcified rPMMA blocks require hard cutting techniques (see Materials and Methods), which are more labor-intensive and produce fewer sections per unit time. Nonetheless, rPMMA sections, in contrast to celloidin, are compatible with high-spatial resolution, multimodal molecular assays—including applications not possible with the traditional workflow (see subsequent paragraphs)—and thus offer the potential for substantially greater data yield and previously unattainable data dimensions (RNA level) per section, an advantage that will likely outweigh reduced sectioning throughput.

Gold-standard equivalent histomorphological preservation of hearing and balance organs in human temporal bone specimens

To evaluate whether the rPMMA method preserves histomorphology on par with the gold-standard celloidin method, we qualitatively compared HE-stained rPMMA sections (Figure 2) to celloidin controls (Supplementary figure S1) from human TBs matched for short postmortem interval (4–7 h) and donor age under 30 years. At low magnification rPMMA section overview, the global tissue architecture was remarkably well preserved across the entire specimen with all anatomical regions appeared intact, undistorted, and in their native spatial relationships (Figures 2A, S1A). Closer views of the cochlear and vestibular organs demonstrated the sensory organs suspended in natural positions in their native fluid-filled compartments, including the cochlear duct (Figures 2B, S1B) and saccule and utricle in the vestibular portion (Figures 2C, S1C), matching celloidin. High-magnification images confirmed excellent cellular preservation, with clearly delineated cytoarchitecture in the organ of Corti (Figures 2D, S1D), spiral ganglion neurons and their axonal projections in Rosenthal's canal (Figures 2E, S1E), and the saccular macula (Figures 2F, S1F). Sensory and supporting cells, as well as neuronal and stromal components, were clearly distinguishable, with preservation quality matching that observed in celloidin-processed specimens. Notably, unlike decalcified celloidin sections, the rPMMA method retains the inorganic (calcium carbonate) matrix of otoconia, permitting direct visualization of these biomineralized crystals within their native tissue context (Figures 2F, S1F). Together, these findings demonstrate that the rPMMA workflow achieves soft tissue preservation equivalent to the histological (celloidin) gold standard.

Preservation of native cochlear implant–tissue interface

To test whether rPMMA embedding combined with hard cutting techniques—i.e. femtosecond laser microtomy and precision diamond wire sawing—maintains the native cochlear implant-tissue interface, we processed a human TB with a cochlear implant electrode array in situ (Figure 3A). Examination of the polymerized block's cut surface showed the

372 silicone-sheathed electrode array in the basal and middle cochlear turns, supported by the rigid
373 resin matrix (Figure 3B). Contact-free femtosecond laser sectioning and abrasive diamond wire
374 sawing then produced sections that preserved the electrode array's genuine positioning within
375 the scala tympani (Figure 3C). At high magnification, multinucleated giant cells—key mediators
376 of the inner ear's foreign-body response[33,34]—were seen lining the silicone sheath,
377 demonstrating preservation of intricate interface details (Figure 3D). Previous histology
378 workflows leverage by our laboratory for human TBs carrying metal implants could not achieve
379 this level of preservation. In the celloidin method, the soft nitrocellulose scaffold cannot support
380 direct cutting of the electrode with steel or tungsten-carbide blades, forcing electrode removal
381 before sectioning and obliterating the tissue–implant interface (Figures S2A–B). Araldite
382 embedding permits cutting with tungsten-carbide blades but still produces displacement and
383 shattering artifacts at the interface (Figures S2C–D) and is incompatible with many downstream
384 molecular assays. To our knowledge, this is the first demonstration of hard-resin embedding
385 paired with advanced sectioning methods that preserves undisturbed cochlear implant–tissue
386 contacts in human temporal bone while remaining compatible with molecular analyses.
387

388 *Improved compatibility with immunohistochemistry and multiplex immunofluorescence*

389 To assess the compatibility of rPMMA-processed human TB sections with antibody-
390 based labeling, we performed chromogenic and multiplexed immunofluorescence labeling
391 following deacrylation. Enzyme-based (chromogenic) immunohistochemistry for osteopontin
392 (OPN) yielded strong, specific labeling of bone matrix within the mineralized otic capsule
393 (Figure 4A), confirming antigen accessibility in the calcified and deacrylated tissue section. In
394 adjacent sections from the same specimen, neurofilament heavy chain (NF-h) robustly labeled
395 spiral ganglion neuron cell bodies (Figure 4B). Multiplex immunofluorescence of a cochlear duct
396 cross-section with antibodies against α-SMA and NF-h (Figure 4C) specifically labeled hair cell

397 stereocilia and auditory nerve fibers in the organ of Corti (Figure 4C, inset), while CellMask and
398 Hoechst 33258 highlighted the exceptionally well-preserved cytoarchitecture in the deacrylated
399 sections. In triple-antibody labeling experiments, we observed strong, specific fluorescence:
400 osteopontin (OPN) intensely labeled the extracellular bone matrix, dentin matrix protein 1
401 (DMP1) specifically marked osteocytes, and type I collagen (Coll I) delineated the fibrous tissue
402 matrix adjacent to the calcified otic capsule (Figure 4D). All negative controls (primary
403 antibodies omitted) were confirmed negative (data not shown). Together, these data
404 demonstrate that deacrylated rPMMA sections of calcified human temporal bone retain epitope
405 integrity across both mineralized and soft tissues. Although we did not conduct a head-to-head
406 comparison with celloidin-processed specimens, our experience shows that
407 immunohistochemistry protocols optimized for FFPE tissues translate reliably to rPMMA-
408 processed sections—unlike with celloidin-processed specimens.
409
410 *High-yield recovery of intact genomic DNA and compatibility with whole-genome sequencing*
411 To assess DNA recovery from rPMMA-processed tissue sections, we extracted genomic
412 DNA from single sections of six human TB specimens with postmortem intervals ranging from
413 4 to 40 hours (mean 16.8 h, SD 6.7 h). The average yield was 15.76 ng per section (SD 18.13
414 ng; Figure 5A), with a mean degradation index of 5.6 (SD 2.5; Figure 5B) and DNA integrity
415 number (DIN) of 2.85 (SD 0.25; not shown). A section with a 40-hour postmortem interval
416 yielded only 1.63 ng of highly degraded DNA. Three celloidin-processed archival control
417 sections yielded negligible DNA amounts (mean 0.005 ng, SD 0.004 ng) and were excluded
418 from downstream analysis. Short tandem repeat (STR) profiling showed full amplification of all
419 17 loci in 60% of rPMMA samples and 16 of 17 loci in the remaining 40%, with no allelic dropout
420 or cross-human contamination (Figure 5C), demonstrating that the rPMMA matrix both
421 preserves native DNA integrity and protects against exogenous (e.g., laboratory staff) DNA

contamination by fully sealing the tissue within the polymerized block. Minimal bacterial contamination was detected (mean 0.47% of reads; SD 0.40%; Figure 5D). These results demonstrate that rPMMA embedding preserves sufficient DNA integrity and yield for downstream molecular analyses in specimens with postmortem intervals below 24 hours.

To determine whether DNA extracted from single rPMMA-embedded sections is suitable for whole-genome sequencing (WGS), we performed WGS directly on DNA from individual tissue sections. Each sample generated approximately 400 million reads, achieving a mean coverage depth of 7.37x (SD 0.70; Figure 5E), with an average duplication rate of 30.8% (SD 8.3%; Figure 5F), consistent with expectations for low-input DNA. Comparison of single nucleotide polymorphism (SNP) variant calls from a matched rPMMA section (TV 7) and a fresh frozen sample (TV 7 FF) from the same specimen showed 75% concordance (Figure 5G), indicating that most true variants are retained despite some dropouts. Saturation analysis indicated a continued increase in variant detection without reaching a plateau for all samples, suggesting that deeper sequencing would further improve yield (Figure 5H). These data confirm that single rPMMA-processed human TB sections are fully compatible with WGS, delivering reliable variant detection and scalable genomic coverage.

Preservation of total RNA species

To evaluate the preservation and in situ accessibility of total RNA species in rPMMA-processed human TB sections—and to compare this with the best-case archival celloidin sections—we performed fluorescent labeling with two RNA-selective dyes (Syto RNASelect and StrandBrite Green). Specimens were matched by postmortem interval (9–10 hours), formalin fixation (6–7 days), and archival storage of less than six months, with celloidin sections kept in 80% ethanol and rPMMA sections stored dry and dark at room temperature. In rPMMA sections, Syto RNASelect yielded nuclear, nucleolar, and cytoplasmic signals in SGNs, a

447 pattern distinctly different from the co-labeled DNA-specific dye Hoechst 33258 (Figure 6A). In
448 contrast, SGNs in celloidin sections exhibited only Hoechst-positive nuclei, with no detectable
449 Syto RNASelect fluorescence (inset, Figure 6A), indicating marked loss of tissue RNA species.
450 To confirm the specificity of the RNA signal in rPMMA tissue, we carried out an on-slide RNase
451 A digest: sections were co-labeled with StrandBrite Green and Hoechst and imaged to establish
452 baseline fluorescence (Figure 6B–B′), then incubated on the microscope stage for 3 hours at
453 room temperature in either RNase A or water (photobleaching control), and finally re-imaged
454 (Figure 6C–C′). After correcting for photobleaching, RNase A treatment caused a significant
455 decrease in nuclear StrandBrite fluorescence (Figure 6B″–B‴), while Hoechst intensity
456 remained statistically unchanged (Figure 6C″–C‴), thereby confirming the in situ specificity of
457 RNA-selective staining in rPMMA-embedded human TB sections.
458
459 *Targeted mRNA integrity confirmed via RNAscope™*
460 We assessed whether the rPMMA workflow and subsequent deacrylation preserve
461 mRNA in human TB sections sufficiently for high-resolution in situ hybridization. Using
462 RNAscope™, we first applied positive controls—PPIB and POLR2A—and a bacterial DapB
463 probe as a negative control. In rPMMA sections, PPIB yielded punctate nuclear signal in non-
464 neuronal cells, while POLR2A signal localized to both nuclei and cytoplasm of SGNs (Figure
465 6D). The bacterial DapB probe produced no detectable signal (Figure 6D′), confirming assay
466 specificity. We then probed for human CALB2 mRNA. Fast Red chromogenic puncta were
467 observed within SGN cell bodies (data not shown) and prominently in vestibular ganglion
468 neurons co-labeled for NF-h, CellMask, and Hoechst (Figure 6E). Quantitative image
469 analysis—segmenting each vestibular ganglion neuron by its NF-h–defined boundary and
470 calculating the fraction of area occupied by CALB2 puncta—revealed marked heterogeneity in
471 CALB2 transcript abundance across individual neurons (Figure 6F). Together, these data

472 demonstrate that rPMMA-processed human TB sections retain mRNA integrity and in situ
473 accessibility, enabling reliable, single-cell–level detection of target transcripts by RNAscope™.
474
475
476 **Discussion**

477 Here, we introduce an innovative histology workflow for calcified human TBs that
478 combines embedding in a rigid PMMA resin with near-serial thin-sectioning via femtosecond
479 laser microtomy and precision diamond-wire sawing. This approach preserves gold-standard
480 morphological detail—on par with the classic celloidin method—while remaining fully
481 compatible with both in situ and sequencing-based molecular assays. By compressing a
482 process that traditionally exceeds 17 months into about six weeks, and by eliminating toxic
483 reagents and high costs, this method provides an unprecedented platform for fully integrated,
484 spatially resolved histo-molecular studies of human auditory and vestibular tissues.

485 Hearing and balance disorders pose a substantial, growing global health burden: over
486 430 million people live with disabling hearing loss, a figure set to exceed 700 million by 2050[35],
487 chronic middle ear infections affect hundreds of millions of children each year[36], and dizziness
488 and vertigo afflict up to 20 percent of adults annually, with a lifetime prevalence around 7–8%[37].
489 Yet in-depth investigation of hearing and balance organ pathologies in the human ear is
490 severely constrained by existing methods—a critical barrier to advancing disease
491 understanding and effective therapies[4]. The century-old, widely adopted celloidin histology
492 workflow preserves exquisite morphology but is largely incompatible with in situ protein and
493 nucleic acid assays[31]; standard formalin-fixation paraffin-embedding (FFPE) supports many
494 molecular assays[38,39], but markedly distorts the human ear's microanatomy, rendering cellular-
495 level interpretation unreliable[23]; and dissociative molecular approaches (e.g. single-cell RNA

496 sequencing) generate rich cell-specific expression profiles, yet sacrifice the three-dimensional
497 tissue architecture critical for spatial contextual insight.

498 Our rPMMA workflow addresses these challenges through several key innovations. Its
499 methacrylate chemistry crosslinks primarily with itself and interacts minimally with endogenous
500 proteins and nucleic acids, preserving biomolecules for downstream analysis. Once cured, the
501 hard, refractive-index–matched resin preserves global and cellular architecture, and
502 immobilizes metallic implants in place. Precision sectioning via contactless femtosecond laser
503 microtomy or abrasive diamond-wire sawing then yields clean, artifact-free slices through both
504 tissue and metal without displacement or distortion. The reversible PMMA matrix can be readily
505 removed with solvent, exposing the tissue for robust, multiplexed immunofluorescence labeling;
506 high-yield, high-quality DNA extraction—while effectively preventing foreign DNA
507 contamination, a common issue with celloidin[28] and paraffin[40]. Library-complexity metrics—
508 including non-saturated sequencing saturation curves and high overlap of unique fragments
509 compared to fresh-frozen controls—demonstrate that even at the modest exploratory read
510 depths we chose, our WGS libraries remain rich in novel content, highlighting the potential for
511 sensitive calling of rare single-nucleotide variants, structural rearrangements, and mosaic
512 mutations. We also successfully performed total RNA in situ labeling and targeted RNAscope
513 for abundant mRNAs, providing proof-of-principle for gene-specific in situ assays on rPMMA-
514 processed human TB sections. Although factors such as postmortem interval, RNA degradation
515 kinetics in different TB tissues, and residual resin removal conditions will need systematic study
516 to define which specimens are amendable for RNA studies, this workflow broadly paves the
517 way for high-resolution, large-scale spatial transcriptomics of human auditory and vestibular
518 tissues. The entire protocol completes in under two months and reduces per-specimen costs
519 by over 90%, enabling truly integrated, spatially resolved histo-molecular investigations of
520 postmortem human auditory and vestibular tissues. Rather than serially sectioning entire

521 specimens, our workflow focuses on producing a select few high-quality sections that each yield
522 rich, high-information molecular data.

523 During method development, we identified three key limitations: (i) *Outgassing during*
524 *polymerization*. PMMA's exothermic free-radical curing can release dissolved gases and
525 residual monomer, generating microscopic bubbles that distort surrounding tissue. We reduced
526 this by using a very slow, multi-stage thermal ramp (from –40 °C to –10 °C, finishing at 4 °C),
527 which mitigates gas evolution during solidification. However, bubbles still form within the bony
528 labyrinth cavities, where they cannot escape. (ii) *Section adhesion and solvent resistance*.
529 Deacrylation requires aggressive solvents (here 2-MEA) that quickly dissolve standard
530 histology glues and dislodge sections. We solved this by mounting 20 µm slices with a two-
531 component Araldite epoxy: it cures to a crystal-clear, solvent-resistant bond that endures hours
532 of solvent exposure. However, its long (hour-scale) cure time limits throughput. Faster UV-
533 curable adhesives may accelerate slide preparation in the future. (iii) *Sectioning throughput and*
534 *accessibility*. Earlier approaches applying diamond sawing to calcified human TBs used wide-
535 blade band saws to cut fixed specimens into millimeter-thick slabs, thereby increasing surface
536 area to accelerate the subsequent decalcification process[41–43]. By contrast, we use 50-80 µm
537 diamond-coated wires to produce thin, ready-to-use sections, and completely bypassing the
538 decalcification step. However, diamond-wire sectioning—and femtosecond laser microtomy—
539 both require specialized equipment and considerable hands-on time, resulting in low-to-
540 moderate throughput. Consequently, these methods are best applied to targeted regions of
541 interest—are less suited to produce (near)serial sections of entire human temporal bone
542 specimens—and deliver single sections that are amendable for high–information–yield
543 molecular assays.

544

545

Conclusion

Here we describe a histology workflow for postmortem human temporal bones that combines gold-standard morphological preservation with versatile, on-section protein and nucleic acid assays—all within a streamlined, cost-effective protocol. This approach establishes a new standard for human tissue spatially resolved molecular studies of hearing and balance disorders using human tissue.

Acknowledgements

We thank Barbara J. Burgess and Diana T. Jones for their decades of technical expertise and stewardship of the human temporal bone collection at Mass Eye and Ear. A.H.E. is grateful to Marcus Müller (University of Tübingen) for early inspiration and invaluable discussions on Technovit® 9100. We thank Daniela Meir and Fabian Baron for their support in harvesting temporal bones during autopsies. This work was funded by the National Institute on Deafness and Other Communication Disorders (NIDCD) National Human Ear Resource Network [U24-DC020849].

562 **References**

563 1. Dillon, C. F., Gu, Q., Hoffman, H. J. & Ko, Ch.-W. Vision, Hearing, Balance, and Sensory
564 Impairment in Americans Aged 70 Years and Over: United States, 1999–2006. *NCHS*
565 *Data Brief* **31**, (2010).
566 2. Maarsingh, O. R., Dros, J., Schellevis, F. G., Van Weert, H. C., Bindels, P. J. & Horst, H.
567 E. V. Der. Dizziness reported by elderly patients in family practice: Prevalence, incidence,
568 and clinical characteristics. *BMC Fam Pract* **11**, (2010).
569 3. World Health Organization. World Report On Hearing. *Human Rights Watch* 1–272
570 (2021).
571 4. Jiam, N. T. & Rauch, S. D. Inner ear therapeutics and the war on hearing loss: systemic
572 barriers to success. *Front Neurosci* **17**, 1169122 (2023).
573 5. Schuknecht, H. Temporal Bone Removal at Autopsy: Preparation and Uses. *Arch*
574 *Otolaryngol* **87**, 129–137 (1968).
575 6. Da Costa Monsanto, R., Pauna, H. F., Paparella, M. M. & Cureoglu, S. Otopathology in
576 the United States: History, Current Situation and Future Perspectives: "The Importance
577 of Otopathology Laboratories." *Otol Neurotol* **39**, 1210 (2018).
578 7. Sagi, V., Kosaraju, N., Moore, L. S., Mulders, J. Y., Solyali, M., Ma, X. et al. Mortui vivos
579 docent: a modern revival of temporal bone plug harvests. *Front Neurosci* **17**, 1242831
580 (2023).
581 8. Lopez, I. A., Ishiyama, G., Hosokawa, S., Hosokawa, K., Acuna, D., Linthicum, F. H. et
582 al. Immunohistochemical techniques for the human inner ear. *Histochem Cell Biol* **146**,
583 367–387 (2016).
584 9. Bauwens, L. J. J. M., Veldman, J. E. & Huizing, E. H. Progress in temporal bone
585 histopathology. *Acta Otolaryngol* **108**, 34–39 (1989).
586 10. Takahashi, M., Kimura, Y., Sawabe, M. & Kitamura, K. Modified paraffin-embedding
587 method for the human cochlea that reveals a fine morphology and excellent
588 immunostaining results. *Acta Otolaryngol* **130**, 788–792 (2010).
589 11. Merchant, S. N., Burgess, B., O'Malley, J., Jones, D. & Adams, J. C. Polyester Wax: A
590 New Embedding Medium for the Histopathologic Study of Human Temporal Bones.
591 *Laryngoscope* **116**, 245 (2006).
592 12. Kimura, R. S., Schuknecht, H. F. & Sando, I. Fine morphology of the sensory cells in the
593 organ of corti of man. *Acta Otolaryngol* **58**, 390–408 (1964).

13. Portmann, D., Fayad, J., Wackym, P. A., Shiroishi, H., Linthicum, F. H. & Rask-Andersen, H. A technique for reembedding celloidin sections for electron microscopy. *Laryngoscope* **100**, 195–199 (1990).
14. Nadol, J. B., Ketten, D. R. & Burgess, B. J. Otopathology in a case of multichannel cochlear implantation. *Laryngoscope* **104**, 299–303 (1994).
15. Thomas, M. B. The Collodion Method in Botany. *Botanical Gazette* **15**, 296–299 (1890).
16. Retzius, G. *Das Gehörorgan der Wirbelthiere: morphologisch-histologische Studien (II.): Das Gehörorgan der Reptilien, der Vögel und der Säugethiere*. (Samson & Wallin, 1884).
17. Schuknecht, H. F. *Pathology of the Ear*. (Harvard University Press, 1974).
18. Nager, G. T. . & Hyams, V. J. . *Pathology of the ear and temporal bone*. (Williams & Wilkins, 1993).
19. Politzer, A. *A text-book of the diseases of the ear for students and practitioners*. (Lea, 1903).
20. Manasse, P. *Handbuch der pathologischen Anatomie des menschlichen Ohres*. (Bergmann, 1917).
21. Miguel-Hidalgo, J. J. & Rajkowska, G. Immunohistochemistry of neural markers for the study of the laminar architecture in celloidin sections from the human cerebral cortex. *J Neurosci Methods* **93**, 69–79 (1999).
22. Keithley, E. M., Horowitz, S. & Ruckenstein, M. J. Na,K-ATPase in the cochlear lateral wall of human temporal bones with endolymphatic hydrops. *Annals of Otology, Rhinology & Laryngology* **104**, 858–863 (1995).
23. O'Malley, J. T., Merchant, S. N., Burgess, B. J., Jones, D. D. & Adams, J. C. Effects of fixative and embedding medium on morphology and immunostaining of the cochlea. *Audiology and Neurotology* **14**, 78–87 (2009).
24. Eckhard, A. H., O'Malley, J. T., Nadol, J. B. & Adams, J. C. Mechanical Compression of Coverslipped Tissue Sections During Heat-induced Antigen Retrieval Prevents Section Detachment and Preserves Tissue Morphology. *Journal of Histochemistry and Cytochemistry* **67**, 441–452 (2019).
25. Bächinger, D., O'Malley, J. T., Wolf, M., Bérnhard, S., Liberman, M. C., Tibbitt, M. W. et al. Poly(Ethylene Glycols) to Facilitate Celloidin Removal for Immunohistochemical Studies on Archival Human Brain and Temporal Bone Sections. *J Histochem Cytochem* (2024) doi:10.1369/00221554241266287.

626 26. Tian, Q., Linthicum, F. H. & Keithley, E. M. Application of labeling techniques to archival
627 temporal bone sections. *Ann Otol Rhinol Laryngol* **108**, 47–53 (1999).
628 27. Ohtani, F., Furuta, Y., Iino, Y., Inuyama, Y. & Fukuda, S. Amplification of RNA from
629 archival human temporal bone sections. *Laryngoscope* **109**, 617–620 (1999).
630 28. McKenna, M. J., Kristiansen, A. G., Tropitzsch, A. S., Tranebjærg, L. & Merchant, S. N.
631 Deoxyribonucleic acid contamination in archival human temporal bones: a potentially
632 significant problem. *Otol Neurotol* **23**, 789–792 (2002).
633 29. Pagedar, N. A., Wang, W., Chen, D. H. C., Davis, R. R., Lopez, I., Wright, C. G. et al.
634 Gene expression analysis of distinct populations of cells isolated from mouse and human
635 inner ear FFPE tissue using laser capture microdissection - a Technical report based on
636 preliminary findings. *Brain Res* **1091**, 289–299 (2006).
637 30. Merchant, S. N. & Nadol, J. B. *Schuknecht's pathology of the ear.* (People's Medical Pub.
638 House-USA, 2010).
639 31. O'Malley, J. T., Burgess, B. J., Jones, D. D., Adams, J. C. & Merchant, S. N. Techniques
640 of celloidin removal from temporal bone sections. *Ann Otol Rhinol Laryngol* **118**, 435–
641 441 (2009).
642 32. Andrews, S. FastQC: A Quality Control tool for High Throughput Sequence Data.
643 https://www.bioinformatics.babraham.ac.uk/projects/fastqc/ (2010).
644 33. Nadol, J. B., Eddington, D. K. & Burgess, B. J. Foreign Body or Hypersensitivity
645 Granuloma of the Inner Ear After Cochlear Implantation: One Possible Cause of a Soft
646 Failure? *Otology and Neurotology* **29**, 1076–1084 (2008).
647 34. Nadol, J. B., O'Malley, J. T., Burgess, B. J. & Galler, D. Cellular immunologic responses
648 to cochlear implantation in the human. *Hear Res* **318**, 11–17 (2014).
649 35. WHO. Deafness and hearing loss. in *Fact Sheet N°300*.
650 36. Conesa, H. R., Skröder, H., Norton, N., Bencina, G. & Tsoumani, E. Clinical and
651 economic burden of acute otitis media caused by Streptococcus pneumoniae in
652 European children, after widespread use of PCVs–A systematic literature review of
653 published evidence. *PLoS One* **19**, e0297098 (2024).
654 37. Neuhauser, H. K., Von Brevern, M., Radtke, A., Lezius, F., Feldmann, M., Ziese, T. et al.
655 Epidemiology of vestibular vertigo: A neurotologic survey of the general population.
656 *Neurology* **65**, 898–904 (2005).
657 38. Michaels, L., Soucek, S. & Liang, J. The ear in the acquired immunodeficiency syndrome:
658 I. Temporal bone histopathologic study. *Am J Otol* **15**, 515–522 (1994).

659 39. Rupp, G. M. & Locker, J. Purification and analysis of RNA from paraffin-embedded
660 tissues. *Biotechniques* **6**, 56–60 (1988).
661 40. Sehn, J. K., Spencer, D. H., Pfeifer, J. D., Bredemeyer, A. J., Cottrell, C. E., Abel, H. J.
662 et al. Occult specimen contamination in routine clinical next-generation sequencing
663 testing. *Am J Clin Pathol* **144**, 667–674 (2015).
664 41. Michaels, L., Wells, M. & Frohlich, A. A new technique for the study of temporal bone
665 pathology. *Clin Otolaryngol Allied Sci* **8**, 77–85 (1983).
666 42. Michaels, L., Gould, S. J. & Wells, M. The microslicing method in the study of temporal
667 bone changes in the perinatal period: An interim report. *Acta Otolaryngol* **99**, 9–14 (1985).
668 43. Huizing, E. H., Veldman, J. E. & Meeuwsen, F. Progress in temporal bone histopathology
669 I. Semithin 3-5 m sectioning of undecalcified human temporal bone after plastic
670 embedding. *Acta Otolaryngol* **99**, 24–28 (1985).
671

672

673 **Figures and figure legends**

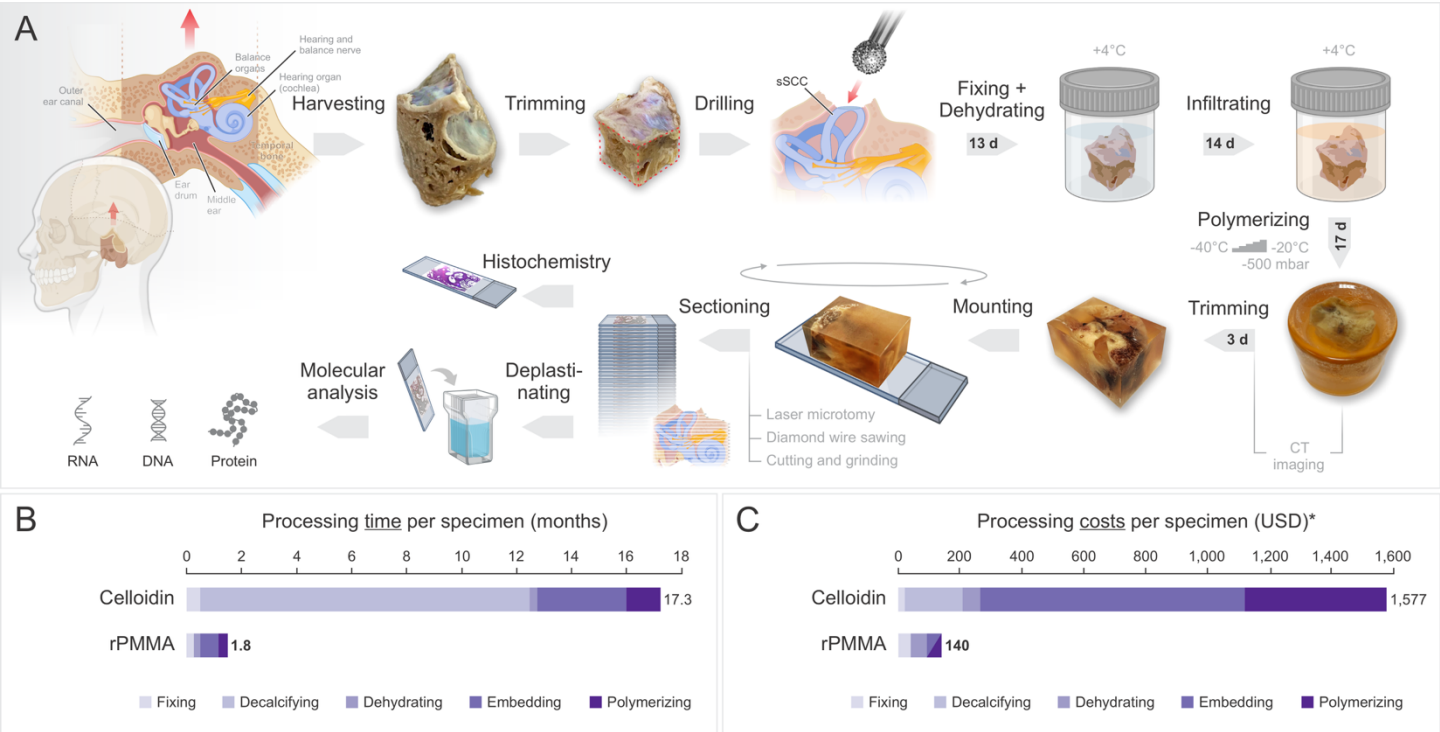

674

675 **Figure 1. rPMMA workflow accelerates TB processing and reduces costs.** (**A**) Tissue
676 processing workflow for non-decalcified human TBs using embedding in a reversible polymethyl
677 methacrylate (rPMMA) resin. (**B**, **C**) Comparison of processing times (B) and costs (C) between
678 the standard celloidin protocol[30] and the rPMMA protocol. sSCC, superior semicircular canal;
679 *, excluding costs for sectioning.

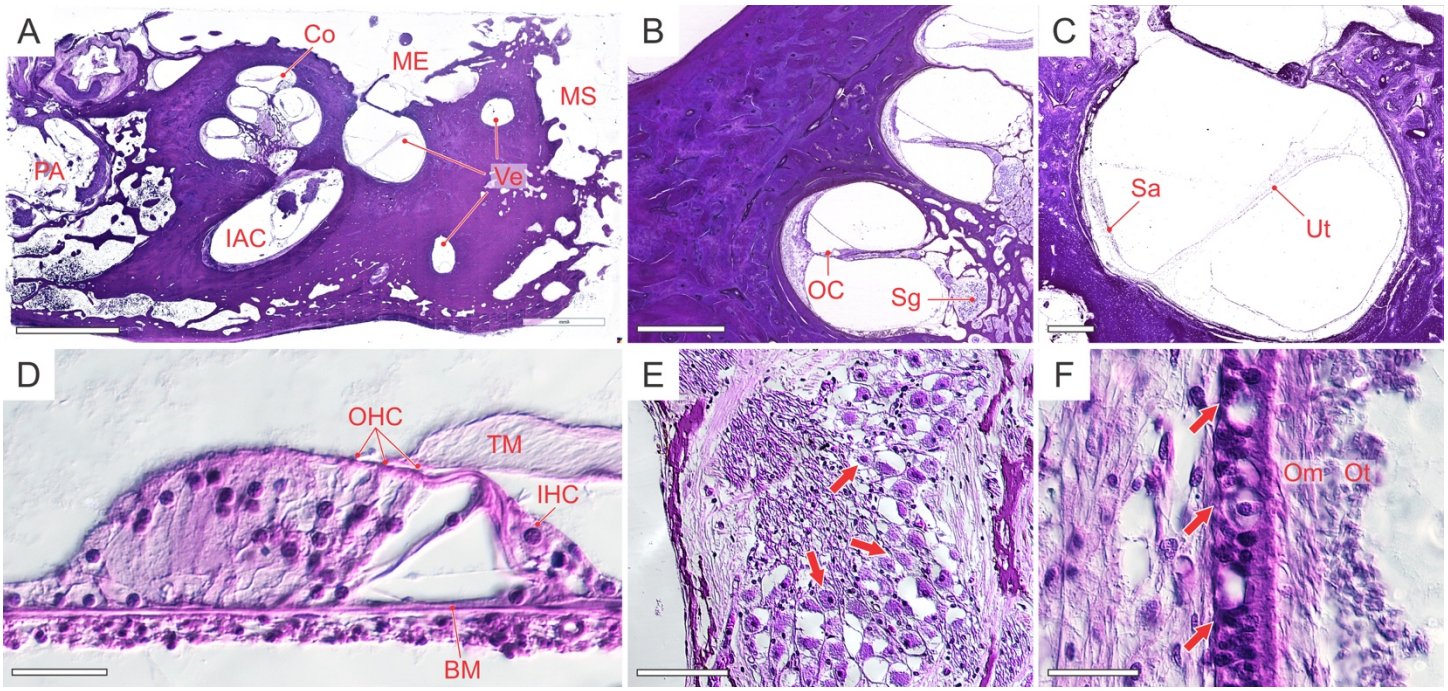

Figure 2. Histomorphology of hearing and balance organs in rPMMA-processed human TBs. (**A**) Overview of hematoxylin/eosin (HE) stained tissue section (Co, cochlea; IAC, internal auditory canal with cochlea-vestibular nerve; ME, middle ear; MS, mastoid space; PA, petrous apex; Ve, vestibule). (**B, C**) Details of the cochlea (B) and the vestibule (C) from (A) (OC, organ of Corti (sensory epithelium); Sg, spiral ganglion (first-order auditory neurons); Sa, saccule, Ut, utricle). (**D – F**) High-power views of Oc (D; BM, basilar membrane; OHC, outer hair cells; IHC; inner hair cells; TM, tectorial membrane), Sg (E; arrows, neuron cell bodies), and Sa (F; arrow, macular epithelium; Om, otoconial membrane; Ot, calcified otoconia (compare to Supplementary figure S1F where Ot are missing). Scale bars: 5 mm (A), 500 µm (B and C), 50 µm (D, E, and F).

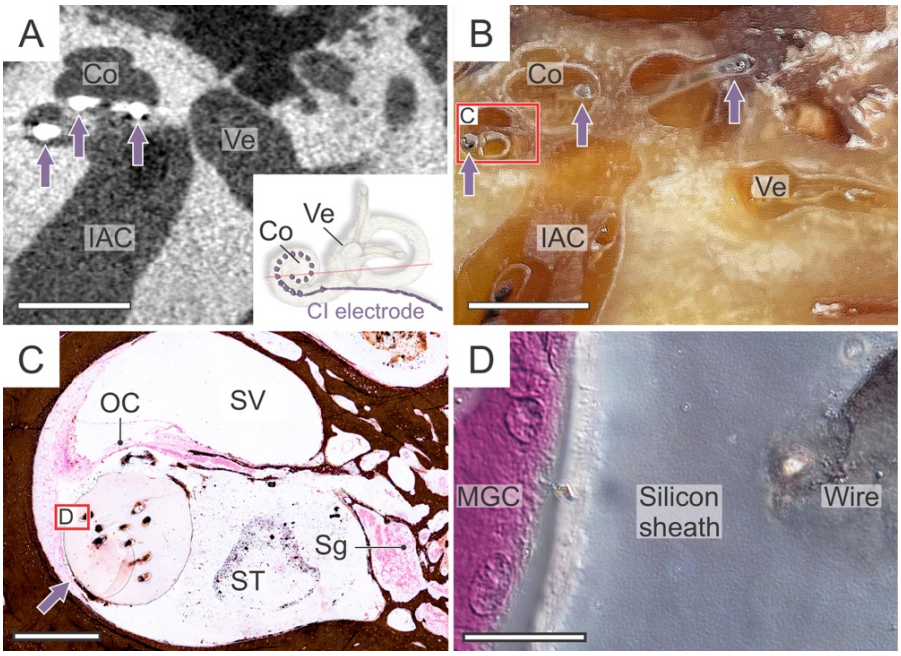

Figure 3. rPMMA-embedded human TB with cochlear implant electrode in situ. (**A**) Axial CT of rPMMA block with embedded TB showing cochlear implant electrode (arrows) in basal and middle turns of the cochlea (Co). Inset: 3D reconstruction of Co, cochlear implant electrode, and vestibular labyrinth (Ve); red line indicates CT imaging plane. IAC, internal auditory canal. (**B**) Cut-surface view of rPMMA block with the embedded TB from (A). Arrows indicate cochlear implant electrode. (**C**) Cross-section of the basal cochlear turn with CI electrode (arrow) in scala tympani (ST). Von Kossa stain highlights calcium-rich bone matrix in brown. SV, scala vestibuli; OC, organ of Corti; Sg, spiral ganglion. (**D**) High-power view of implant-tissue interface (location indicated in (C)) showing a multinucleated giant cell (MGC) abutting the electrode's silicon sheath. Scale bars: 5 mm (A, B), 500 μm (C), 50 μm (D).

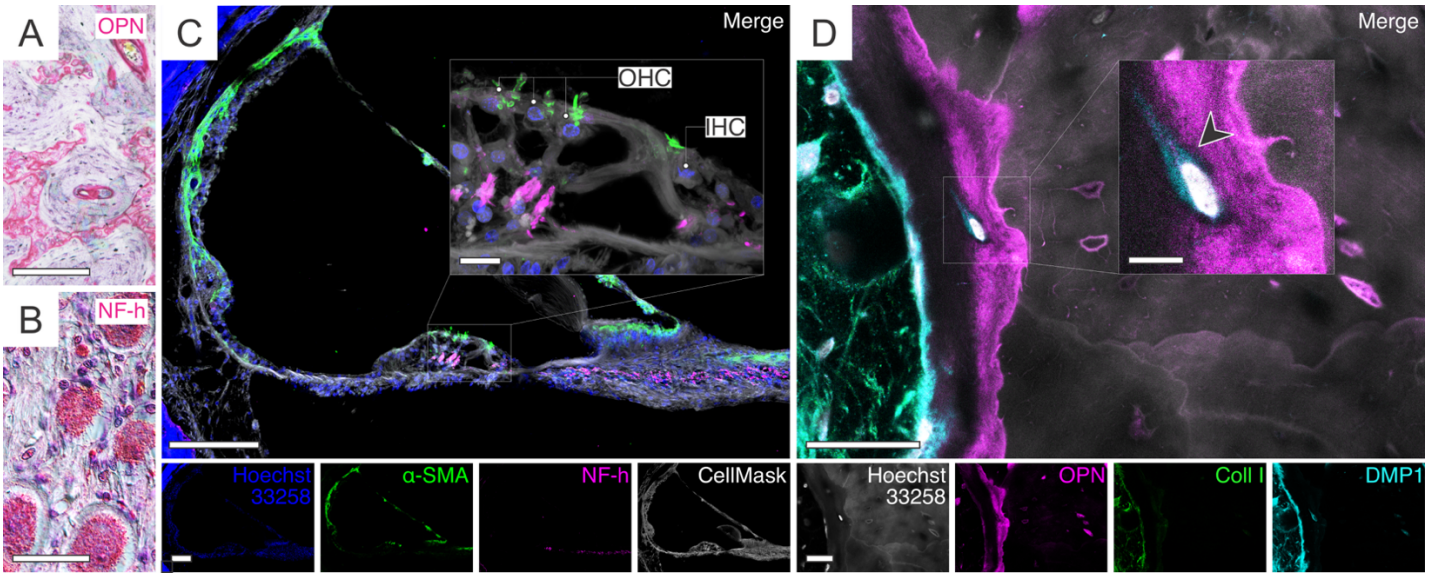

Figure 4. Immunohistochemistry in rPMMA-embedded human TB sections. (**A, B**) Enzyme (alkaline phosphatase)-immunohistochemistry for osteopontin (OPN) outlines structures (globuli interossei) in otic capsule bone (A); neurofilament-heavy (NF-h) labels spiral ganglion neuron cell bodies (B); nuclei counterstained with HE. (**C**) Immunofluorescence for alpha-smooth muscle actin (α-SMA; green), NF-h (magenta), CellMask (white), and Hoechst 33258 (blue) in a cochlear duct cross-section; inset shows organ of Corti with OHC and IHC. (**D**) Immunofluorescence for OPN (magenta), collagen I (Coll I; green), and dentin matrix protein-1 (DMP1; cyan) with Hoechst 33258 (blue) in the calcified otic capsule bone and adjacent fibrous tissue. Scale bars: 200 μm (A), 50 μm (B), 200 μm (C), 50 μm (D), 10 μm (insets, C and D).

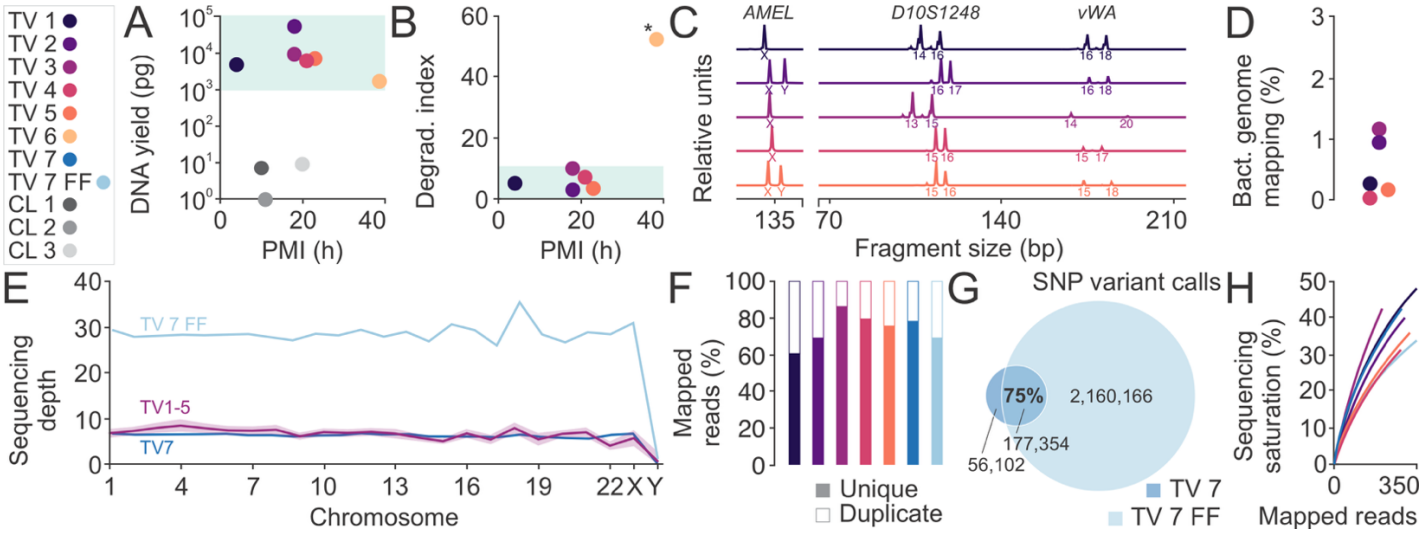

Figure 5. DNA Extraction and WGS Metrics from rPMMA- vs. Celloidin-Embedded human TBs. (**A–B**) DNA yield (A) and integrity (B) in relation to the postmortem interval (PMI) *, TV 6 (PMI 40 h) was excluded due to extensive DNA degradation. (**C**) Representative short tandem repeat (STR) profiles at at the X-chromosomal AMEL locus and autosomal D10S1248 and vWA loci. (**D**) Bacterial genome mapping for TV 1-5. (**E**) Average sequencing coverage across the genome: TV 1-5 (purple), TV 7 (blue), and a fresh-frozen (FF) control from the same donor as TV 7 (cyan). (**F**) Sequencing saturation curves based on unique mapped reads. (**G**) Counts of unique versus duplicate mapped reads for each sample. (**H**) Sequencing saturation curves for TV 1-7 and TV 7 FF.

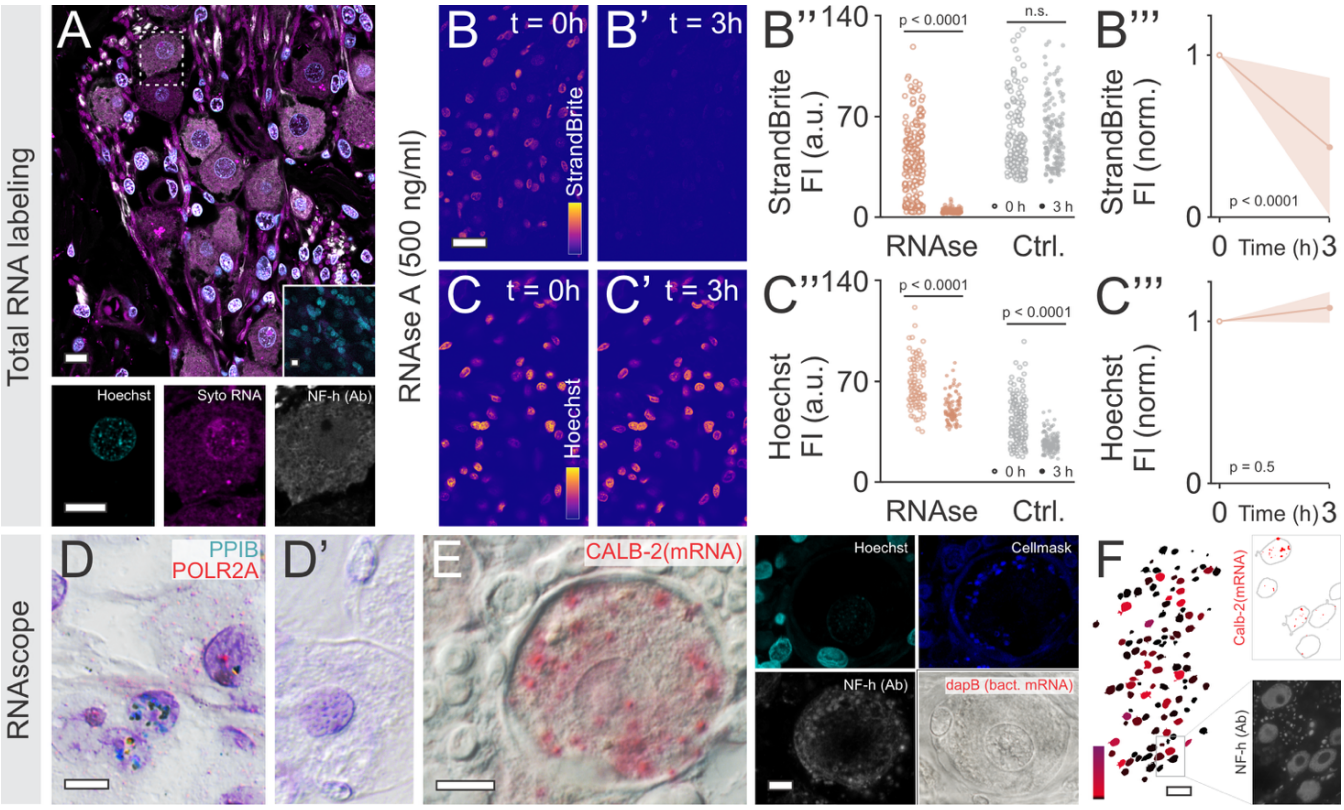

Figure 6. Total RNA in situ labeling and RNAscope™ in rPMMA- versus celloidin-processed human TBs. (**A**) Syto RNAselect (RNA-selective; magenta) and Hoechst 33258 (DNA-selective; blue) fluorescent labeling in rPMMA-embedded spiral ganglion cells (SGNs), with neurofilament-heavy (NF-h, white). Inset: SGNs in celloidin section. No Syto RNAselect labeling observed. (**B-C'''**) StrandBrite (RNA-selective; B–B''') and Hoechst 33258 (C–C''') in SGNs at 0 min (B, C) and after 3 h (B', C') digestion with RNase A (500 ng/ml) versus control (DEPC-water only). Fluorescence intensity (FI) for StrandBrite (B'') and Hoechst 33258 (C''), and corresponding decay slopes (B''', C'''). (**D, D'**) Chromogenic RNAscope™ targeting housekeeping mRNAs PPIB and POLR2A in SGNs (D) and bacterial (dabP) negative control (D'). (**E, F**) Chromogenic RNAscope™ for Calbindin-2 (Calb-2) mRNA (E, red) combined with fluorescent NF-h (green), CellMask™ membrane stain, and Hoechst (blue); bacterial negative control inset. (F) Quantification of Calb-2–positive area in 100 NF-h^{+} vestibular ganglion neurons. Scale bars: 10 µm (A), 20 µm (B–C'), 10 µm (D–E), 100 µm (F).

Supplementary figures and figure legends

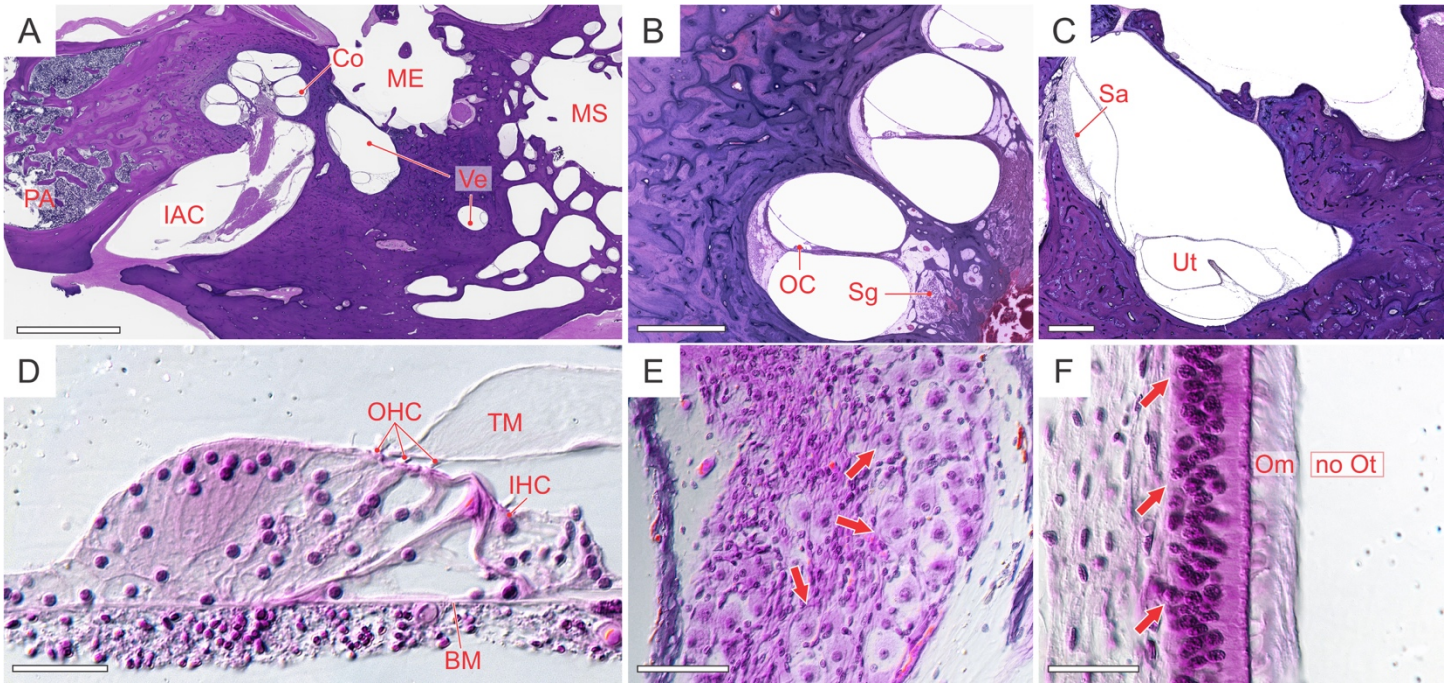

Supplementary figure S1. Histomorphology of hearing and balance organs in celloidin-processed human TBs. (**A**) Overview of hematoxylin/eosin (HE) stained tissue section (Co, cochlea; IAC, internal auditory canal with cochlea-vestibular nerve; ME, middle ear; MS, mastoid space; PA, petrous apex; Ve, vestibule). (**B, C**) Details of the cochlea (B) and the vestibule (C) from (A) (OC, organ of Corti (sensory epithelium); Sg, spiral ganglion (first-order auditory neurons); Sa, saccule, Ut, utricle). (**D – F**) High-power views of Oc (D; BM, basilar membrane; OHC, outer hair cells; IHC; inner hair cells; TM, tectorial membrane), Sg (E; arrows, neuron cell bodies), and Sa (F; arrow, macular epithelium; Om, otoconial membrane; no Ot, otoconia missing due to prolonged decalcification (compare to Figure 1F). Scale bars: 5 mm (A), 500 µm (B and C), 50 µm (D, E, and F).

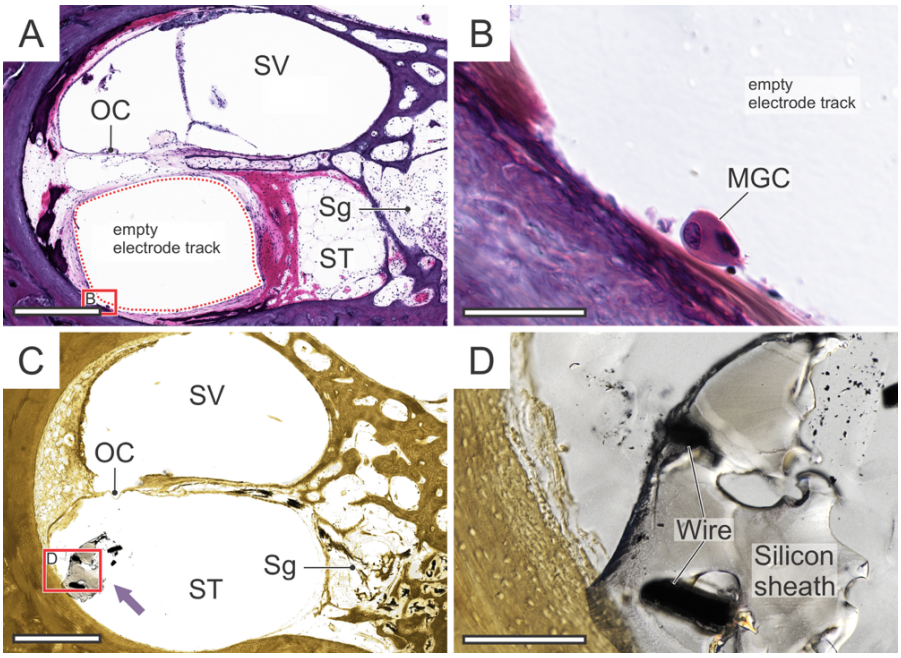

Figure S2. Human TBs processed in celloidin (A, B) or araldite (C, D). In celloidin-embedded specimens the CI electrode was removed prior to decalcification, yielding an empty track in the scala tympani (ST) of the basal cochlear turn: (**A**) low-power cross-section showing ST and scala vestibuli (SV) (OC, organ of Corti; Sg, spiral ganglion); (**B**) high-power view of the empty track with a multinucleated giant cell (MGC). In Araldite-embedded specimens the electrode remained in situ: (**C**) cross-section of the basal turn with the CI electrode (arrow) in ST; (**D**) high-power view showing electrode damage and displacement caused by steel-blade microtome sectioning. Scale bars: 50 µm (A, C); 50 µm (B, D).

Supplementary table S1. Primary and secondary antibodies used for immunostaining.

Primary AB	Working dilution	Cat. #, Vendor	Linked secondary AB (+ tertiary link)	Working dilution	Cat. #, vendor	Figure
Rabbit anti-osteopontin	1 :50	SC21742, Santa Cruz	KA-50F, Universal Alkaline Phospatase Immunostaining Kit (for mouse and rabbit primary antibodies), Diagnostic Biosystems			4A
Rabbit anti-neurofilament heavy	1 :160	N4142, Sigma				4B
Mouse anti-alpha smooth muscle actin	1 :200	A2547, Millipore Sigma	Donkey anti-mouse IgG (H+L) Alexa 488	1 :400	715-545-150, Jackson ImmunoResearch	4C
Rabbit anti-neurofilament heavy	1 :500	N4142, Millipore Sigma	Donkey anti-rabbit IgG (H+L) Alexa 568	1 :400	711-575-152, Jackson ImmunoResearch	4C
Rabbit anti-osteopontin	1 :250	ab8448, Abcam	Donkey anti-rabbit IgG (H+L) Alexa 568	1 :400	711-575-152, Jackson ImmunoResearch	4D
mouse anti-collagen I		ab21286, Abcam	Donkey anti-mouse IgG (H+L) Alexa 488	1 :400	715-545-150, Jackson ImmunoResearch	4D
Sheep anti-dentin matrix protein 1	1 :100	AF4386, R&D Systems	Biotinylated donkey anti-sheep IgG (H+L) + Streptavidin Alexa 647	1 :400 1 :800	713-065-147, Jackson ImmunoResearch 016-600-084, Jackson ImmunoResearch	4D

Supplementary material 1: Technovit® 9100 Embedding Protocol for Calcified Human Temporal Bones

1. Personal protective equipment (PPE) & safety procedures

- Lab coat, nitrile gloves, and safety goggles
- Handle volatile or caustic chemicals (formalin, Histo-Clear™, all Technovit® 9100 Kit solutions) in a certified fume hood.
- Use face shield and cryogenic gloves when handling solutions or specimens at temperatures below –20 °C.
- Have appropriate spill kits readily available.
- Follow institutional safety and chemical waste disposal protocols; adapt as needed.

2. Reagents & Solutions

- Fixatives & Solvents
  - 10% neutral buffered formalin or 4% paraformaldehyde
  - Ethanol (50%, 70%, 80%, 95%, 100% [200 proof])
  - Histo-Clear™ (orange oil–based xylene substitute)
- Embedding Kit
  - Technovit® 9100 Embedding Kit (Ted Pella, Inc. #813-900)
  - Heavy paraffin oil (Supelco PX0046-1)
- Chromatography & Destabilization
  - Aluminum oxide (Al_2O_3), 99% (Fisher Scientific AA4717136)
  - Chromatography column with PTFE stopcock (Fisher 31-500-983)

3. Preparing Technovit Solutions

- Destabilized Base Solution (dBS):
  - Fill chromatography column with 50 g Al_2O_3 powder.
  - Add ~710 mL base solution (BS) to column.
  - Collect ~700 mL filtrate (= dBS) at ~1 drop/s into a brown glass bottle.
- Pre-infiltration Solutions:
  - PIS 1: 100 mL BS + 100 mL Histo-Clear™
  - PIS 2: 200 mL BS + 0.5 g Hardener 1
  - PIS 3: 200 mL dBS + 0.5 g Hardener 1
- Infiltration Solution (IS):
  - 200 mL dBS + 0.5 g Hardener 1 + 16 g poly methyl methycrylate (PMMA) powder
- Polymerization Solutions (PS):
  - PS-A: 230 mL dBS + 0.4 g Hardener 1 + 36.8 g PMMA
  - PS-B: 25 mL dBS + 2 mL Hardener 2 + 1 mL Regulator
- Storage: Keep all solutions at –20 °C until use. Equilibrate at +4 °C before use.

4. Specimen Processing Schedule

	Solution	Conditions	Pressure	Duration
Fixing	Fixative	+4°C	ambient	3 days
Dehydrating	Ethanol 50%	+4°C		1 day
	Ethanol 70%	+4°C		1 day
	Ethanol 80%	+4°C		1 day
	Ethanol 95%	+4°C		1 day
	Ethanol 95%	+4°C		1 day
	Ethanol 100% (200 proof)	+4°C		1 day
	Ethanol 100% (200 proof)	+4°C		1 day
	Histo-Clear™	+4°C		1 day
	Histo-Clear™	+4°C		1 day
Infiltrating	Pre-infiltration solution 1 (PIS 1)	+4°C		3 days
	Pre-infiltration solution 2 (PIS 2)	+4°C		3 days
	Pre-infiltration solution 3 (PIS 3)	+4°C		3 days
	Infiltration solution (IS)	+4°C		4 days
		-40°C		1 day
Polymerizing	Polymerization solution (PS) • Mix 90 ml PS-A + 10 ml PS-B in a 4 oz glass jar; leave the jar open (do not screw the lid on). • At **-40°C**, turn the specimen **daily** onto each of its 6 sides to release gas bubbles. • On the **first day at -30°C**, orient specimen in final position, pour a layer of **paraffin oil** on top of the polymerization solution.	-40°C	-500mbar	5 days
		-30°C		3 days
		-25°C		3 days
		-20°C		2 days
		-15°C		2 days
		+4°C		2 days
			Total	**43 days**

5. Detailed Polymerization Steps

- Chill specimen in IS at –40 °C (final day of infiltration).
- Pre-cool PS-A, PS-B, glassware, and vacuum desiccator to –40 °C.
- In fume hood, mix 90 mL PS-A + 10 mL PS-B in a pre-chilled jar; place open in the desiccator.
- Transfer specimen into mixed PS; turn on all six faces daily at –40 °C to release bubbles; re-evacuate to ~–500 mbar.
- From day 6 onward (–30 °C stage), leave sealed; do not open until polymerization completes.
- At end of –15 °C stage, test surface hardness; if still soft, cap jar and store at +4 °C for 2 days.

6. Post-Embedding Workflow

- Wrap glass jar with fully polymerized resin in cloth or large piece of paper, using safety glasses safety gloves and in a container, carefully fracture glass with e.g. a hammer and extract embedded block.
- Polymerized blocks can be stored at room temperature.
- Continue with block trimming and then thin sectioning using precision diamond wire sawing or laser microtomy.